IEEE Access
Multidisciplinary | Rapid Review | Open Access Journal

Received December 10, 2018, accepted January 1, 2019, date of publication January 11, 2019, date of current version February 4, 2019.

Digital Object Identifier 10.1109/ACCESS.2019.2892130

Experimental Verifications of Low Frequency Path Gain (*PG*) Channel Modeling for Implantable Medical Device (IMD)

SHUANG ZHANG[1,2,3], (Student Member, IEEE), SIO HANG PUN[1], (Senior Member, IEEE), PENG UN MAK[2,4], (Senior Member, IEEE), YU PING QIN[3], YI HE LIU[3], YUE MING GAO[5,6], (Member, IEEE), AND MANG I VAI[1,2], (Senior Member, IEEE)

[1]State Key Laboratory of Analog and Mixed-Signal VLSI, University of Macau, Macau 999078, China
[2]Department of Electrical and Computer Engineering, Faculty of Science and Technology, University of Macau, Macau 999078, China
[3]College of Computer Science, Neijiang Normal University, Neijiang 641100, China
[4]Department of Chemical Engineering and Biotechnology, University of Cambridge, Cambridge CB3 0AS, U.K.
[5]Key Laboratory of Medical Instrumentation and Pharmaceutical Technology of Fujian Province, Fuzhou University, Fuzhou 350116, China
[6]College of Physics and Information Engineering, Fuzhou University, Fuzhou 350116, China

Corresponding author: Peng Un Mak (fstpum@um.edu.mo)

This work was supported in part by the Science and Technology Development Fund of Macau under Grant 024/2009/A1, Grant 093/2015/A3, and Grant 088/2016/A2, in part by the University of Macau under Grant MYRG2018-00146-AMSV, Grant MYRG2016-00157-AMSV, and Grant MYRG2015-00178-AMSV, in part by the Neijiang Normal University through the Leading Talent Training Project under Grant 2017[Liu Yi-He], in part by the Neijiang Normal University through the Innovative Team Program under Grant 17TD03, in part by the Foundation of Ph.D. Scientific Research of Neijiang Normal University under Grant RSC201704, in part by the Sichuan Province Academic and Technical Leader Training Funded Projects under Grant 13XSJS002, in part by the Foundation of Ph.D. Scientific Research of Neijiang Normal University under Grant 2019[zhang shuang] and Grant 2019[wang jiujiang], in part by the National Natural Science Foundation of China under Grant U1505251 and Grant 61201397, in part by the Project of Chinese Ministry of Science and Technology under Grant 2016YFE0122700, and in part by the Project of Fujian S&T Department under Grant 2018I0011.

ABSTRACT With the development of microelectronics and sensor technologies, implantable electronic devices are employed in many applications. These devices are distributed on or in the human bodies and are used to transmit signals wirelessly to external equipment. In conventional wireless communications, the antennas need a lot of space and power, and their strong electromagnetic interference limits the available locations for implantable devices. In the more recently developed galvanic coupling intra-body communication technology, human tissues are used as the media of signal transmission, and this method has therefore been applied to resolve the spatial limitations of conventional wireless communications methods. This paper presents a mathematical model of multi-layer galvanic coupling based on the volume conductor theory to analyze the transmission mechanism of these implantable intra-body communication devices. The proposed model is based on the quasi-static approximation conditions of Maxwell's equations, the field and potential are solved from Poisson's equation, and an equation was obtained to model the channel attenuation. The channel gain in a model of human limbs can be used to calculate within the frequency range of lesser than 1 MHz. To verify the accuracy and applicability of the model, the computed results were compared with the physiological saline and porcine tissue experimental results in the 100-kHz frequency.

INDEX TERMS Implantable communication, galvanic coupling intra-body communication, Poisson's equation, volume conductor theory, implantable medical device (IMD).

I. INTRODUCTION

Research on implantable medical electronic monitoring and control devices has attracted much interest because implantable medical electronic devices can be used not only to monitor human health indicators, but also to treat certain diseases such as epilepsy and tetraplegia [1]–[3], and to replicate the functions of some organs, as with the cardiac pacemaker and the artificial cochlea. However, the signal transmission efficiency of the implantable devices has been an important research question. Although many communica-

tion methods have been proposed in the past several decades, the many restrictions associated with these methods have made only very few of them available for use in cardiac pacemakers, deep brain stimulators, gastric defibrillators, and other medical electronics [4]–[8].

Communication systems can be classified as either wired or wireless transmission. In wired communications, the wires connecting the implantable and external devices must pierce through biological tissues, which often cause tissue infection or other complications. In addition, when the living body moves, the connecting wire introduces some noise that lowers the signal-to-noise ratio [9]. The wireless communications (electromagnetic coupling [1], [10], [11], and intra-body [12] communications) can help to solve some problems by the wired communications. Because of the higher bandwidths, electromagnetic coupling and radio frequency communications have higher communication frequencies; therefore, they can achieve higher communication speeds. However, human tissues produce a strong shielding effect against high-frequency signals, resulting in significant signal attenuation. Furthermore, high-frequency radiation may cause injury to human tissues, and a larger implantation space is required to hold the communication antenna [5]. Therefore, the radio frequency communications are unsuitable for implantation in the brain, bone marrow, or thoracic cavity.

In galvanic coupling intra-body communication, human tissues become the signal transmission medium, avoiding interference because no complicated connecting wires are used. This method also avoids the need to implant a communication coil or antenna because the signal couples directly with the human body. Furthermore, galvanic coupling intra-body communication occurs at communication frequencies of less than 1 MHz with little radiation [20]. For these reasons, this communication method can be used for devices implanted in almost any part of the body.

To facilitate the study of the signal transmission mechanism in galvanic coupling intra-body communication and provide theoretical support for the communication channel, several theoretical models have been proposed, including simplified circuit [13]–[16], numerical solution [17]–[19], and analytical solution [20] models. The simplified circuit model is based on a simplified model in which human tissues are considered to be electronic components [13]–[16]. This modeling method is easily implemented with simple calculations; however, any variation in channel parameters such as the communication frequency [13]–[15], implanted depth [16] and communication distance, and then the properties of the electronic components must be redefined and applied in a new derivation of the model, so the simplified circuit model is poor repeatability. Therefore, the results of this method are unsatisfactory for analysis of multi-frequency implantable intra-body communication channels.

In channel modeling, numerical solutions model [17]–[19] are often chosen because the subject's portion used in channel modeling (such as human body) cannot be approximated by a simple geometrical shape. As a consequence, numerical techniques (such as Finite Element method (FEM)) are often chosen for solving the channel modeling problem instead of the analytical solution. This is especially true for the iterative algorithms since they are very sensitive to the shape of the object. However, analytical solutions can still be used with good effect when noniterative algorithms are applied since they are less sensitive to the shape of the object.

Therefore, in the existing numerical solution models, structural simplification is always reasonably used to reduce the sensitivity of the models to geometric structures. The analytic solution is feasible when the geometric structure is not very sensitive. PUN's [20] showed that when the human forearm was simplified to a multi-layer cylinder, the result of the analytical solution model approximates the experimentally obtained result. Therefore, the analytical solution model can be applied to the analysis of multi-frequency implantable intra-body communication channels.

In addition, the analytical solution can also be used to quickly and effectively analyze the influence of physical quantities upon the model and analyze the intermediate process of calculation; moreover, analytical solutions can provide the basis for both non-iterative and iterative algorithms. They also have some significant advantages compared with a numerical method.

The analytical solution model demonstrates better repeatability than the simplified circuit model and, unlike the numerical solution model, its calculation is independent of the interpolation function and element resolver. Therefore, the sensitivity matrix can be well constructed, and the calculation is not computationally expensive.

As mentioned above, every modeling method has its advantages and disadvantages, and the realization of numerical solution in the implantable channel modeling is very excellent. However, in the case of relatively simple geometry and complex parameter variations, the analytical solution is more advantageous. Since we expect to analyze the effect of every small parameter change on the signal transmission in the channel, the numerical solution is difficult to be fast in achieving the calculation due to the parameters change. Therefore, in this study, we choose analytical solution.

In the case of signal transmission from the inner to outer part of the body, the internal excitation signal may be considered to originate in the biological tissue. For the research problem presented in this paper, most of the previous literatures have focused on the simplified circuit and numerical solution models, and therefore a simple mathematical model is needed to explain this problem.

In this paper, the authors propose a multilayer mathematical model of an implantable intra-body communication channel based on the volume conductor theory. Section II presents the proposed analytical solution model based on the volume conductor theory under the quasi-static electromagnetic field condition and the source field Poisson's equation. Section III validates the accuracy and reasonability of the model by comparing the mathematical solutions for a single-layer model

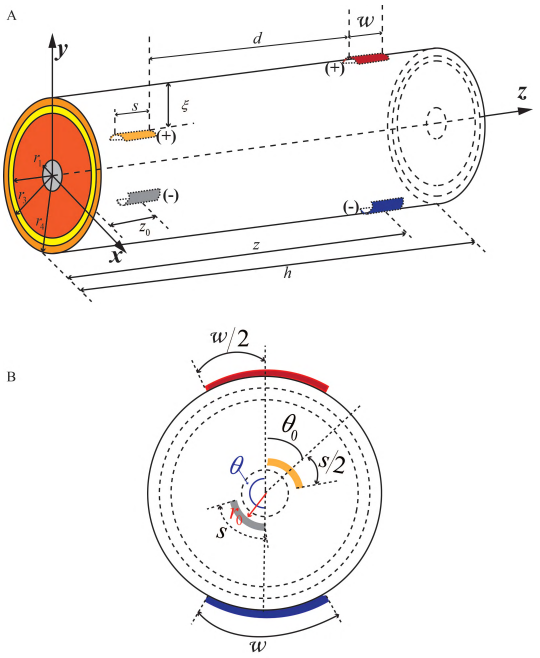

FIGURE 1. Simplified implantable multi-layer volume conductor model with the finite separation d and numerable layers, in which the signal source and source electrodes can be implanted at any position in any layer in the model.

and a multi-layer model with experiments in a physiological saline and porcine tissues. Section IV discusses some of the limitations affecting the results obtained in Section II and III, and Section V presents conclusions.

II. METHODS

A. MATHEMATICAL MODEL

As stated in [15]–[21], the geometric structure of a human limbs can be considered as a multi-layer cylindrical volume conductor formed by skin, fat, muscle, cortical and cancellous bone. Therefore, the research object of a limb is considered to be a multi-layer cylinder with length h and maximum radius r_N. This geometric structure is shown in Figure. 1. In a cylindrical coordinate system; the research object can be described as a cylinder (r, θ, z) that satisfies the volume conductor theory. Within this cylindrical coordinate system, the signal source is a pair of electrodes with the size $s \times s \times d_0$ or $w \times w \times d_0$ (d_0 is the source electrode thickness) that are installed in any layer of the cylinder with positions (r_0, θ_0, z_0) and $(r_0, \theta_0 + \theta, z_0)$, respectively, where (r_0, θ_0, z_0) and $(r_0, \theta_0 + \theta, z_0)$ denotes the position of the signal source (Positive electrode or negative electrode locations). The radii of the cylinder's for different layers from inside to outside are $(r_1, r_2, \cdots, r_{N-1}, r_N)$,where r_1 is the innermost layer, r_N is the outermost layer. To simplify the model, the electrical characteristics of the tissues are considered to be isotropic, and the conductivity and relative permittivity in the corresponding layers are $(\sigma_1, \sigma_2, \cdots, \sigma_{N-1}, \sigma_N)$ and $(\varepsilon_1, \varepsilon_2, \cdots, \varepsilon_{N-1}, \varepsilon_N)$, respectively.

Under the quasi-statics condition from [22], the electric potential distribution of the volume conductor may be expressed as

$$\nabla \cdot \vec{J} = -\nabla \cdot (\widetilde{\sigma}_s \vec{\nabla} \varphi) = \vec{I} \tag{1}$$

where $\vec{J}$ is the current density $(A \cdot m^{-2})$ applied to the limb through the implantable device; $\widetilde{\sigma}_s$ is the complex conductivity; φ represents the potential within the human limb; and $\vec{I}$ is the volume current density $(A \cdot m^{-3})$ in the signal source, expressed as

$$\widetilde{\sigma}_s = \sigma_s + j\omega\varepsilon_0\varepsilon_s, \quad s = 1, 2, \cdots, N-1, N \tag{2}$$

where σ_s is the conductivity of the s-layer tissue and ε_s is the permittivity of the s-layer tissue. In the cylindrical coordinate system, each layer of the cylinder r is a homogeneous isotropic conductor [23]. Therefore,

$$\frac{1}{r}\frac{\partial}{\partial}(r\frac{\partial \varphi}{\partial r}) + \frac{1}{r^2}\frac{\partial^2 \varphi}{\partial \theta^2} + \frac{\partial^2 \varphi}{\partial z^2} = -\frac{\vec{I}}{\widetilde{\sigma}_s}\delta(r - r_0)\delta(\theta - \theta_0)\delta(z - z_0) \tag{3}$$

On the basis of the Fourier series expansion equation of the δ-function [23], [24], (3) can be expressed as

$$\begin{cases} \frac{1}{r}\frac{\partial}{\partial}(r\frac{\partial g_{sm}}{\partial r}) - (\frac{m^2}{r^2} + \frac{n\pi^2}{h^2})g_{sm} = -\frac{1}{\widetilde{\sigma}_s}\delta(r - r_0) \\ \delta(\theta - \theta_0) = \frac{1}{2\pi}\sum_{m=1}^{\infty} e^{jm(\theta - \theta_0)} \\ \delta(z - z_0) = \frac{2}{h}\sum_{n=1}^{\infty} sin(\frac{n\pi z}{h})sin(\frac{n\pi z_0}{h}) \end{cases} \tag{4}$$

where g_{sm} is the Radial function, h is the volume conductor length.

B. BOUNDARY AND CONTINUITY CONDITIONS

In order to derive the model solution in the volume conductor, the model should also satisfy the boundary conditions [23], [24] presented in this section.

$$\nabla^2 g_{sm}(r \mid r_0) = 0 \tag{5}$$

$$\frac{\partial \varphi(r, \theta, z)}{\partial r} \mid_{r=r_N} = 0 \tag{6}$$

$$\varphi_s(r_s{}^+, z) = \varphi_s(r_s{}^-, z) \tag{7}$$

$$\vec{J}_s(r_s{}^+, z) = \vec{J}_s(r_s{}^-, z) \tag{8}$$

And assumption:

$$\varphi(r, \theta, z) \mid_{z=0} = \varphi(r, \theta, z) \mid_{z=h} = 0 \tag{9}$$

In the cylindrical volume conductor, when the electrode center $r_0 \neq r_N$, The implanted electrode is not located on the surface of volume conductor.

C. RADIAL FUNCTION

The model solution can be derived on the basis of the boundary conditions of the volume conductor represented by (5)-(9). To simplify the calculation, the Radial Function can be derived:

$$g_{sm}(r \mid r_0) = A_{sm}I_m(kr) + B_{sm}K_m(kr) + \begin{cases} \frac{1}{\widetilde{\sigma}_{source}} K_m(kr_0)I_m(kr), & 0 < r \le r_0; \\ \frac{1}{\widetilde{\sigma}_{source}} I_m(kr_0)K_m(kr), & r_0 < r < r_N; \end{cases} \tag{10}$$

where $k = n\pi/h, n = 1, 2, \cdots, \infty$; $\widetilde{\sigma}_{source}$ is the complex conductivity of the layer where the signal source was located. A_{sm} and B_{sm} denote the coefficients of the $I_m(kr)$ and $K_m(kr)$, divided by $r = r_0$, respectively; I_m is the modified Bessel function of the first kind of order m and K_m is the modified Bessel function of the second kind of order m.

D. POTENTIAL DISTRIBUTION MODEL

By solving the mathematical model with (3)-(10), an analytical potential solution for the potential distribution model can be expressed as:

$$\begin{aligned} \varphi_s(r, \theta, z) &= -\frac{4\vec{J}}{\pi^2} \sum_{s=1}^{N} \sum_{m=1}^{\infty} \sum_{n=1}^{\infty} [\frac{1}{m} sin(m\triangle) e^{im(\theta-\theta_0)}] \\ &\quad \times sin\frac{n\pi z}{h} [\frac{1}{n} sin\frac{n\pi z_0}{h} sin\frac{n\pi w/2}{h}] [A_{sm}I_m(kr_s) \\ &\quad + B_{sm}K_m(kr_s) + \frac{1}{\widetilde{\sigma}_{source}} \psi(kr_s)] \\ &= \widetilde{J}\tau_s(r, \theta, z) \end{aligned} \tag{11}$$

where

$$\psi(kr_s) = \begin{cases} K_m(kr_0)I_m(kr_s) & 0 < r_s \le r_0 \\ I_m(kr_0)K_m(kr_s) & r_0 < r_s < r_N, \end{cases}$$

$\widetilde{J}$ is the current constant (current density), there $\widetilde{J} = -\frac{4\vec{J}}{\pi^2}$; φ_s represents the potential within the human limb in s-layer; $\tau_s(r, \theta, z)$ is the volume conductor constants (include geometric constants, electrical characteristic constants and implantable constants), $\triangle = W_1/2r_{source}$ and W_1 is the electrode width (s or w), r_{source} is the radii of the layer where the signal source was located.

E. PATH-GAIN MODEL

From potential distribution model, the path gain PG model can be expressed as:

$$\begin{aligned} G(r, \theta, z) \mid_{dB} &= 20log_{10}(\varphi_{RX}(r, \theta, z)/\varphi_{TX}(r_0, \theta, z_0)) \\ &= 20log_{10}(\widetilde{J}\tau_{RX}(r, \theta, z)/\widetilde{J}\tau_{TX}(r_0, \theta, z_0)) \\ &= 20log_{10}(R(r)) + 20log_{10}(\Phi(\theta)) \\ &\quad + 20log_{10}(Z(z)) \\ &\quad - 20log_{10}(\tau_{TX}(r_0, \theta, z_0)) \end{aligned} \tag{12}$$

where τ_{RX} is the receiver volume conductor constant, τ_{TX} is the transmitter volume conductor constant,

$$R(r) = \sum_{s=1}^{N} \sum_{m=1}^{\infty} [A_{sm}I_m(kr_s) + B_{sm}K_m(kr_s) + \frac{1}{\widetilde{\sigma}_{source}} \psi(kr_s)]; \tag{13}$$

$$\Phi(\theta) = \sum_{m=1}^{\infty} [\frac{1}{m} sin(m\triangle) e^{im(\theta-\theta_0)}]; \tag{14}$$

$$Z(z) = \sum_{n=1}^{\infty} sin\frac{n\pi z}{h} [\frac{1}{n} sin\frac{n\pi z_0}{h} sin\frac{n\pi w/2}{h}]; \tag{15}$$

III. VERIFICATION OF THE PROPOSED MODEL

In the experiment, we performed each set of experiment for continuous four days, and every day three groups of data were measured as the experimental results of this sample. According to the variation property of the image, we selected 12 groups' experimental data to fit the experimental results. By fitting, we got the fitting (the distance and the depth using the least square model (the highest second power), the angle variation using the Lorentzian peak model) curve of the experimental results.

Three parameters of the model will be verified, it is the implantation depth ξ ($\xi = r_N - r_0$) of the device, the distance d ($d = z - z_0 - \frac{s+w}{2}$) of the implanted device in z direction and the intersection angle θ_0 between the electrode at the transmitting end and that at the receiving end on the $x - y$ section. In the experiment, two parameters were set as constants, and the other one as variable. Meanwhile, in order to facilitate calculation, the intersection angle between θ the positive electrode at the transmitter and the negative electrode at the receiver is defined as a constant ($\theta = 180^o$).

A. PHYSIOLOGICAL SALINE EXPERIMENT

In order to verify the accuracy of the model, physiological saline was selected as the medium for preliminary verification. First, we used a transparent plastic cylindrical bottle with a diameter of 80mm and a height of 170mm as the experimental sample vessel. At a height position of 10mm, two square openings of $20\times20mm^2$ were cut, with centers symmetrical in relation to the center of the cylinder, and these openings were used to set the receiving electrodes. Two square copper electrodes subjected to a glass insulation treatment were inserted in the bottle's neck for use as the signal electrode. The copper electrode size was length$\times$width$\times$thickness:$20\times20\times1mm^3$; The signal cable wick glass tube cladding of thickness 0.25 mm, and its overall length was 150mm, which was open at two ends to input the current signal and fix the signal electrode. This experimental layout was shown in Figure.2.

In the experiment, we injected physiological saline with the conductivity and permittivity of $\sigma = 1.75\ S/m$ and $\varepsilon_r = 80.4$ at the frequency of 100 kHz [19], respectively, into the cylindrical plastic bottle. Because the electric conductance property was the same throughout the physiological saline, the liquid in the bottle may be regarded as an

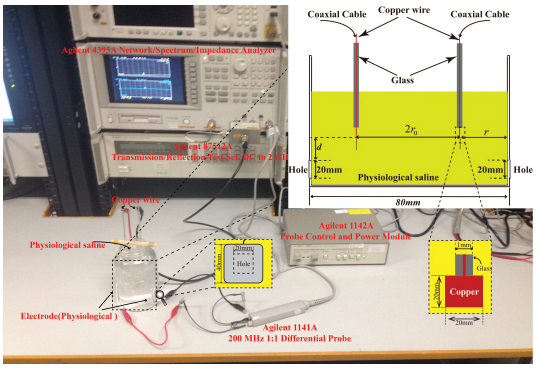

FIGURE 2. Schematic of the physiological saline experiment.

TABLE 1. Physiological saline experiment parameters.

	r_0[mm]	θ_0[deg]	z[mm]	results
Distance	15	0	0∼80	Figure. 3
Depth	5∼20	0	30	Figure. 4
Angel	15	0∼180	30	Figure. 5

*$r_N = 40mm, \theta = 180^o, \xi = r_N - r_0$

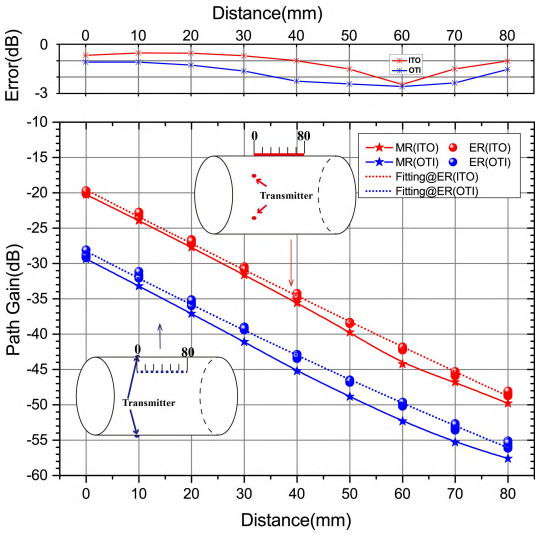

FIGURE 3. Physiological saline experiment results and models results (distance as variable).

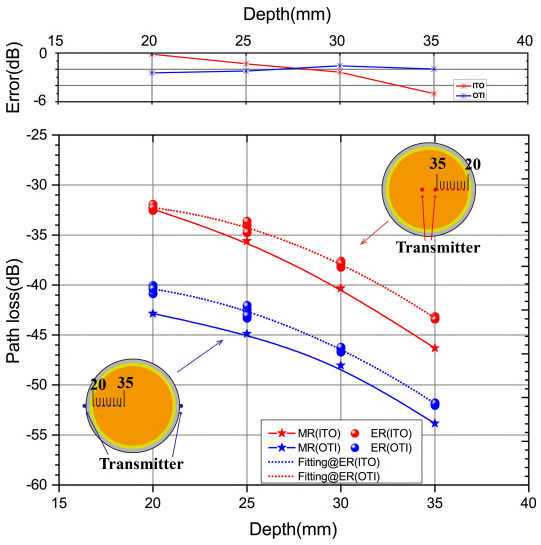

FIGURE 4. Physiological saline experiment results and models results (depth as variable).

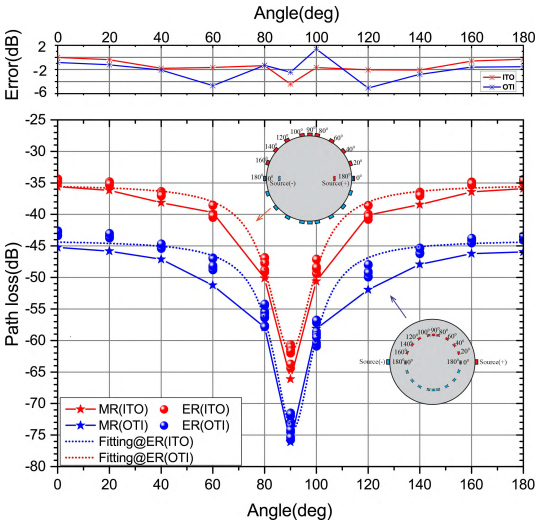

FIGURE 5. Physiological saline experiment results and models results (angle as variable).

isotropic single layer. The conductivity and the permittivity of the physiological saline were substituted into the established analytical solution model.

In the system, two copper electrodes were used as the transmitter (signal source) and receiver, the transmitter input current density was $\vec{J}$, and $\vec{J}$ may be expressed as follows:

$$\vec{J} = \begin{cases} \vec{J}_{source} & if \quad \theta_0 - \triangle < \theta < \theta_0 + \triangle \\ 0 & other\ wise \\ -\vec{J}_{source} & if \quad \pi + \theta_0 - \triangle < \theta < \pi + \theta_0 + \triangle \end{cases} \tag{16}$$

In which $\vec{J}_{source} = I/S$; I is the injected current (A), S is the electrode area (m^2).

In the experiment, the transmission distance (d), the implantation depth (ξ) and the transmitter and receiver angle (θ_0), assuming that two parameters were set as constants, and the other one was varied. (shown in Table 1), we analyzed the path gain characteristics of the channel. Figure. 3 to Figure.5 show the experimental results and *PG* model results with those from the proposed model when the signal transmits from inside to outside (ITO) and from outside to inside (OTI).

According to the experimental bottle geometrical parameters and physiological saline conductivity and permittivity, equation (12) was used to gain the calculated result; from the controlled experimental results (ER) of single layer volume conductor and the model calculation results (MR) in Figure. 3 to in Figure. 5, we found that, difference between

MR and ER are usually lower than 5dB at the same position in the same repeated experiments. However, it was found from these figures that, the overall variation tendency of the experimental result, are consistent. It is concluded from the fitting experimental and model result that, whether the signal was transmitted from outside to inside (OTI) or from inside to outside (ITO), R-squares of the experimental result and the fitting curve were larger than 0.977 (the R-squares of the experimental result and the fitting curve with respect to distance and depth were larger than 0.995). This was shown that the fitting result is identical with the experiment result in the single-layer volume conductor controlled experiment, and the fitting curve result can explicate the experimental result effectively.

ERROR

In order to verify accuracy of the fitting curve of the experimental results compared with the *PG* model results, we selected the error of two curves for contrast, it is expressed as:

$$G_{error} = G_{model} - G_{fitting} \tag{17}$$

where G_{model} is the computed result of the PG model; $G_{fitting}$ is the computed result of the fitting curve derived from the experimental results.

From the error between the model result and the fitting result, we found that the error between the two results in the single-layer volume conductor experiment is -6dB to 2dB (only -2.5dB to -0.5dB in the distance experiment) and the absolute error is smaller than 6dB. Furthermore, the variation tendency of the curve is approximate consistent. Therefore, in the distance model of the single-layer experiment, the model which we propose can explain the channel transmission characteristics of the implantable intra-body communication effectively.

However, human tissues are unlike normal saline which has only single ingredient and structure. It is known that main tissues composing human geometric construction include skin, fat, muscle and skeleton, and they form human body through the complex envelope structure. In order to study the property of the model with complicated tissue characteristics, we design the Muscle with Bone Effect Experiment.

B. MUSCLE WITH BONE EFFECT EXPERIMENT

1) SINGLE-LAYER EXPERIMENT

In order to study transmission characteristics of signals in animal body tissues, on the basis of the physiological saline experiment, we replaced experimental samples with minced porcine muscle tissue. To avoid the influence of the fat on the communication channel, in selecting the samples, we selected muscle tissues from the same part (e.g., buttock) of a pig as the experimental samples. Prior to this experiment, some enmeshed fat in the muscle was first removed so that the entire sample consisted of muscle (muscle: 95%). After the fat removal, the muscle was minced in a meat grinder and then filled in the empty bottle (diameter: 100*mm*, height: 235*mm*). At a position 40*mm* away from the bottom, two square openings of $20\times20mm^2$ were cut, with centers that were symmetrical in relation to the center of the cylinder, and these openings were used to set the receiving electrodes. At the bottom of the bottle, the 30 *mm* high blue part is the hollow base; in filling, it is filled up with minced muscle tissue. Because all of the filler was the minced muscle tissue, the transmission channel could be considered to be a single-layer isotropic communication channel (muscle) (see Fig.6). The experimental method was the same as that of the physiological saline experiment.

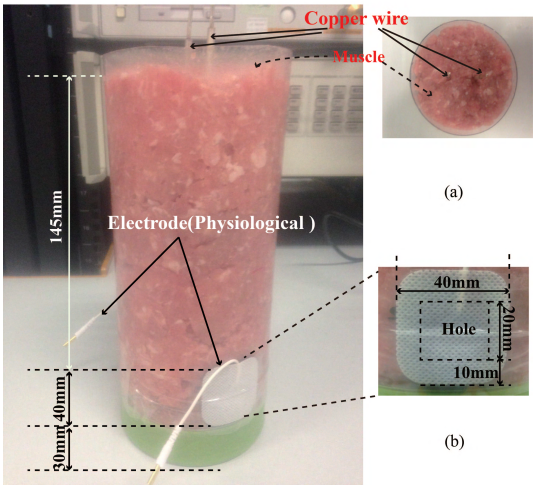

FIGURE 6. Experiment schematic of the Single-layer experiment.

A 0 dBm sinusoidal signal of 100 kHz was input to the implantable signal electrode and surface electrode. The conductivity and permittivity of the minced muscle we selected were $\sigma = 0.25\ S/m$ and $\varepsilon_r = 9900$ at the frequency of 100 kHz [29]–[32], respectively. When the signal transmitted from inside to outside (ITO) the tissue, the source electrode radius was equal to 10 *mm* ($r_0 = 10\ mm$), the receiver electrode radius is equal to located at 50 *mm*.

In the experiment, the transmitter and receiver angle is a constant ($\theta_0 = 0$), assuming that the transmission distance (d) (or the implantation depth (ξ)) as a constant, and the other one was varied. (shown in Table 2) we analyzed the path gain characteristics of the channel.

TABLE 2. Single-layer experiment parameters.

	r_0[mm]	θ_0[deg]	z[mm]	results
Distance	15	0	50∼130	Figure. 7
Depth	5∼35	0	60	Figure. 8

*$r_N = 50mm, \theta = 180^o, \xi = r_N - r_0$

Comparisons of the experimental result and the model calculation result of single-layer volume conductor with muscle characteristics are shown in Figure. 7 and Figure. 8. Although we try to reduce the gap by re-filling, the electrodes in two different experiments inevitably have some differences and this certainly causes larger error than in the salt-water experiment.

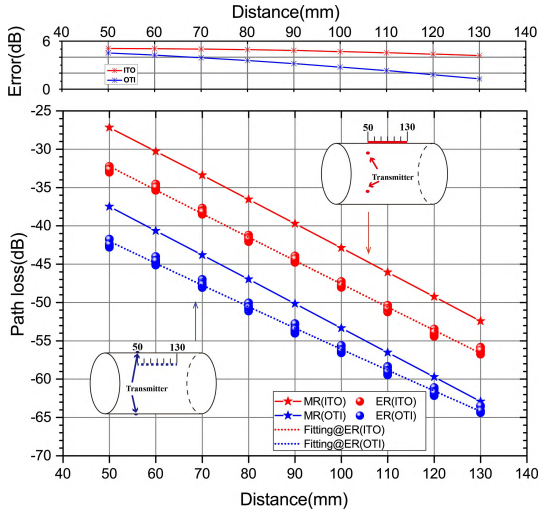

FIGURE 7. Single-layer experiment results and models results (distance as variable).

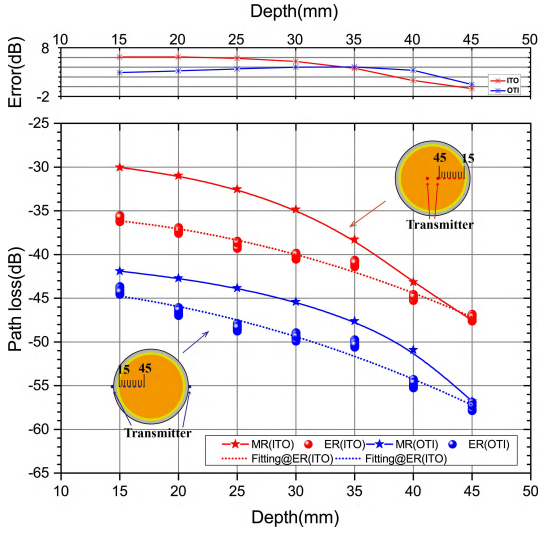

FIGURE 8. Single-layer experiment results and models results (depth as variable).

According to the fitting experiment result, it is concluded that, whether the signal is transmitted OTI or ITO, R-squares of the experiment and the fitting curve are larger than 0.996. Almost all points are close to the fitting curve. The overall change curve of the experiment result is nearly consistent with that of the fitting curve, so the fitting curve can show fully variation tendency of the channel in the experiment. By comparing, the error between the model result and the fitting result ranges from 1.1dB to 5.3dB, so the model is valid. However, in the depth experiment, although R-squares of experimental result and the fitting curve are also larger than 0.963, the experimental result at some positions deviate seriously from the fitting result. Although the overall changing curves in the two groups of results are nearly consistent with the fitting curve, the fitting curve can also explain variation tendency of the channel in the experiment. By comparing the model result

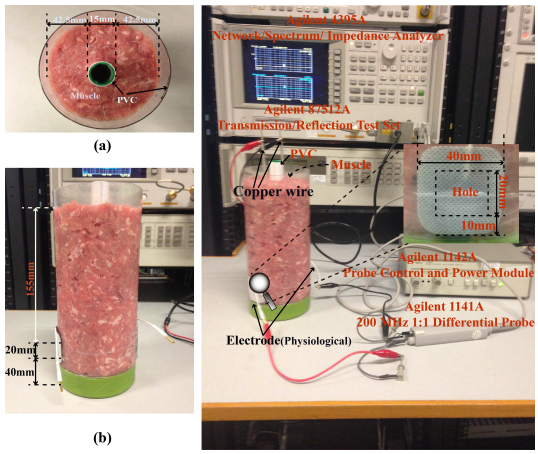

FIGURE 9. Experiment schematic of the Bi-layer experiment.

we proposed with the fitting result, the error between two groups of results ranges from −0.5dB to 6.2dB. This model is available. By contrast, the result of the distance experiment is more consistent with the model calculation result.

2) BI-LAYER EXPERIMENT

On the basis of the Single-layer experiment, we use a polyvinyl chloride (PVC 235-mm-long) Water pipe as the bone (see Figure.9). The experimental method was the same as that of the Single-layer experiment. In the experiment, because all of the filler was the minced muscle tissue, the transmission channel could be considered to be a bi-layer isotropic communication channel (Hollow).

In this experiment, assuming that the transmission distance (d) (or the implantation depth (ξ)) as constants, by changing the implantation depth (ξ)(or the transmission distance (d)) (shown in Table 3), we analyzed the path gain characteristics of the channel.

TABLE 3. Bi-layer experiment parameters.

	r_0[mm]	θ_0[deg]	z[mm]	results
Distance	15	0	50∼130	Figure. 10
Depth	5∼35	0	60	Figure. 11

*$r_N = 50mm, \theta = 180^o, \xi = r_N - r_0$

Compared with the experimental result and the model calculation result of the bi-layers of volume conductor with skeleton effect are shown in Figure. 10 and Figure. 11, the experimental result is not changed significantly because the conductive medium is still muscle. Although we find the data in the depth experiment result are close to the fitting curve, in each repeated experiment, the electrode is difficult to occupy the electrode position in the previous experiment; therefore, the experiment result has a large error (about 2dB), and R-square of the fitting curve becomes relatively smaller (less than 0.91). However, the model result we proposed and the fitting result have a basically consistent variation tendency.

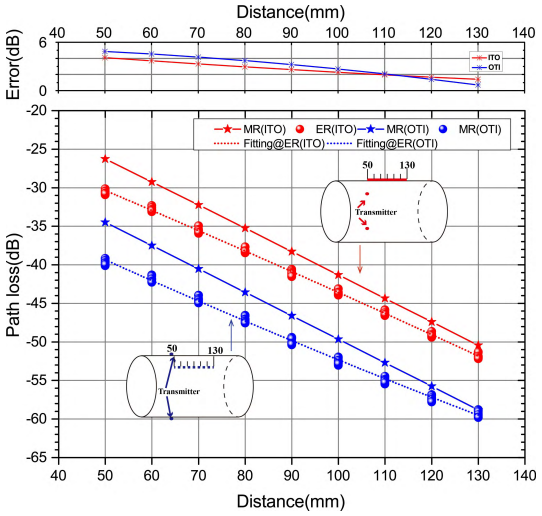

FIGURE 10. Bi-layer experiment results and models results (distance as variable).

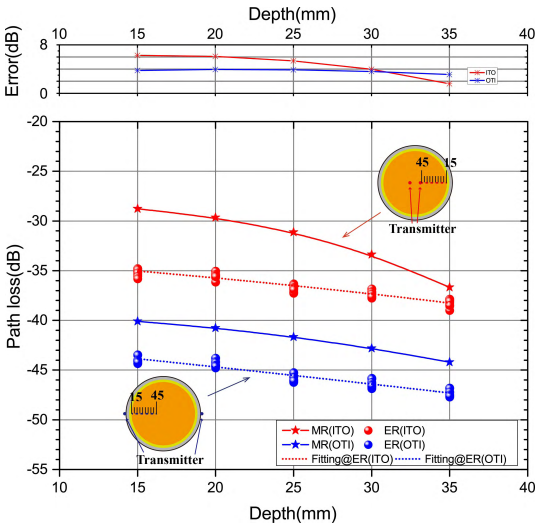

FIGURE 11. Bi-layer experiment results and models results (depth as variable).

3) MULTI-LAYER EXPERIMENT

In order to study the path loss characteristics of the model in a complex channel, we used porcine tissues to construct a cylindrical phantom (Figure. 12). In this experiment, we first selected a piece ($230mm \times 360mm$) of rectangular pigskin with fat, and then a uniform thickness of $5mm$ was achieved through surgical dissection. Measurements showed that the skin thickness was $2mm$ and the fat thickness was $3mm$ in the rectangular pigskin, and these were considered to be the dimensions of the skin layer and the fat layer of the phantom. The pigskin was rolled into a circular ring with a height of $215mm$, and stitched together with surgical sutures to form a barrel shape (Figure. 12). The three-layer prosthesis was fabricated by filling the gap between the bone and muscle with 2500 g of minced muscle tissue. The conductivity and permittivity of the skin and fat we selected were

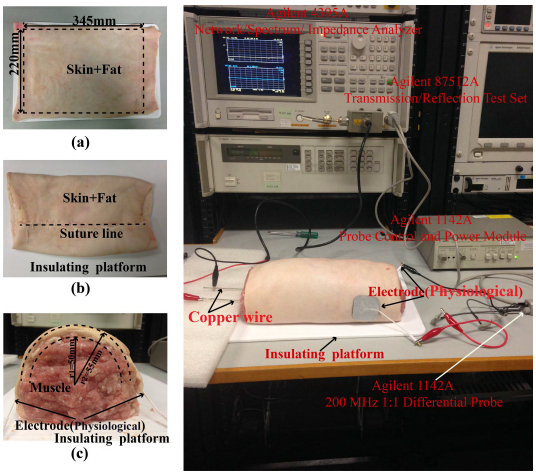

FIGURE 12. Experiment schematic of the multi-layer experiment.

TABLE 4. Multi-layer experiment parameters.

	r_0[mm]	θ_0[deg]	z[mm]	results
Distance	15	0	50∼130	Figure. 13
Depth	5∼35	0	60	Figure. 14

*$r_N = 50mm, \theta = 180^o, \xi = r_N - r_0$

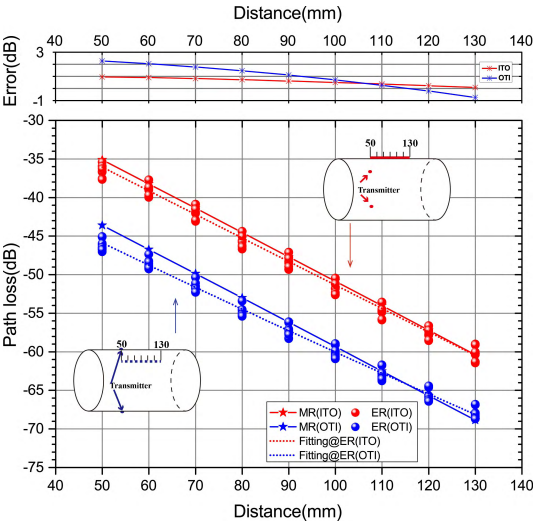

FIGURE 13. Multi-layer experiment results and models results (distance as variable).

$\sigma = 0.00016\ S/m$, $\varepsilon_r = 965$ and $\sigma = 0.003 S/m$, $\varepsilon_r = 98$ at the frequency of 100 kHz [29]–[31], respectively.

The square copper electrodes used in the single-layer experiment and the two-layer experiment were inserted in the phantom to replace the implantable device. In this experiment, when the transmission distance (d) (or the implantation depth (ξ)) as constants, the implantation depth (ξ) (or the transmission distance (d)) was varied to analyze channel path gain characteristics. (show in Table 4).

According to the single-layer conductor experiment and the bi-layer conductor experiment with skeleton effect, compared with the experimental result and the model calculation result of the multilayer volume conductor in Figure. 13 and Figure. 14, because skin and fat are taken into account,

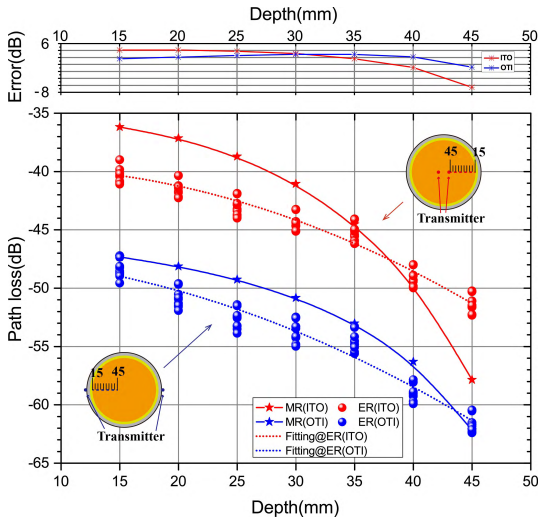

FIGURE 14. Multi-layer experiment results and models results (depth as variable).

channel attenuation is greatly changed (averagely increased by −5dB). Meanwhile, because complexity of channel tissues is heightened, this causes the error (up to 4dB) of the repeated experiment at the same position which is further increased under the same condition. According to curve fitting, we conclude that the R-square of the fitting curve is larger than 0.989 in measurement of the distance experiment and the R-square is larger than 0.937 in measurement of the depth experiment. The data of the experimental results are close to the fitting curve. This shows that the variation tendency of the fitting curve can fully explain the experimental results. By comparing the fitting result and the model calculation result, we find that the error (−1dB to 2.2dB) between two groups of curves is obviously reduced in the distance experiment, but curve intersection occurs, this shows that the variation tendency has changed. This phenomenon becomes more distinct in the depth experiment, in which there is evident curve intersection and the error (−7.5dB to 4.2dB) between two groups of curves is obviously raised. By contrast, it can be seen that the result of the distance experiment and the model calculation result have better consistency.

IV. DISCUSSION

In the Section III of the paper, accuracy and performance of the mathematical model were analyzed through the in vitro experiment . In the in vitro experiment, we selected physiological saline for initial validation (Figure. 3 to Figure.5). By comparing the measured result and the calculated result, it was concluded that the model's calculated result was highly identical to the experimental data.

In the Muscle with Bone Effect Experiment (from single-layer experiment to multi-layer experiments), it can be seen that the distance experiment obviously has better consistency with model calculation than the depth experiment. This is because distance setting of the electrode is controlled more easily than depth setting. As a whole, the errors between many

TABLE 5. Physiological saline experiment fitting parameters.

Fitting	Distance experiment (Figure. 3)			
Equation	$y = b_0 + b_1 * x^1 + b_2 * x^2$			
Mode	ITO		OTI	
RSS	10.87215		17.5869	
R-Square	0.99885		0.99795	
	Value	SE	Value	SE
b_0	-19.56335	0.0755	-28.2622	0.09602
b_1	-0.38606	0.0044	-0.38849	0.0056
b_2	2.59408E-4	5.29294E-5	5.07832E-4	6.73184E-5
Fitting	Depth experiment (Figure. 4)			
Equation	$y = b_0 + b_1 * x^1 + b_2 * x^2$			
Mode	ITO		OTI	
RSS	3.93563		4.0323	
R-Square	0.99516		0.99536	
	Value	SE	Value	SE
b_0	-40.96171	1.25629	-47.0644	1.27162
b_1	1.10361	0.09422	0.95996	0.09537
b_2	-0.03344	0.00171	-0.03134	0.00173
Fitting	Angle experiment (Figure. 5)			
Equation	$y = y_0 + (\frac{2A}{\pi})(\frac{w}{4(x-x_c)^2+w^2})$			
Mode	ITO		OTI	
RSS	1.44734		1.89268	
R-Square	0.9787		0.97714	
	Value	SE	Value	SE
y_0	-35.2591	0.14599	-44.08814	0.1634
x_c	90.07807	0.1841	90.96593	0.18473
w	20.55902	0.49573	18.61137	0.47489
A	-854.95061	19.94384	-873.82676	21.04128
H	-26.47395	0.3628	-29.89008	0.43567

*SE:Standard Error,RSS:Residual Sum of Squares, RCS:Reduced Chi-Sqr

TABLE 6. Single-layer experiment fitting parameters.

Fitting	Distance experiment(Figure. 7)			
Equation	$y = b_0 + b_1 * x^1 + b_2 * x^2$			
Mode	ITO		OTI	
RSS	16.4373		17.62182	
R-Square	0.9975		0.99677	
	Value	SE	Value	SE
b_0	-16.55678	0.50308	-27.21662	0.5209
b_1	-0.31717	0.01181	-0.30327	0.01223
b_2	6.9075E-5	6.50811E-5	1.43952E-4	6.73852E-5
Fitting	Depth experiment(Figure. 8)			
Equation	$y = b_0 + b_1 * x^1 + b_2 * x^2$			
Mode	ITO		OTI	
RSS	25.43816		54.87794	
R-Square	0.97809		0.96344	
	Value	SE	Value	SE
b_0	-35.61177	0.59701	-43.31211	0.87688
b_1	0.07341	0.0428	0.00975	0.06287
b_2	-0.00734	7.06041E-4	-0.00709	0.00104

*SE:Standard Error, RSS:Residual Sum of Squares

experiments at the same position also remain in the acceptable range (less than 5dB). The experimental result, the fitting result and the model calculation result change at the same order of magnitude, and their curves coincide well.

In the multi-layer experiment, because both the fat layer and the skin layer are thin (skin layer: 2mm; fat layer: 3mm), it is difficult to place electrodes on them to carry experiments. Therefore, in the depth experiment, the minimum skin depth we designed is 15mm. Meanwhile, in the single-layer and bi-layer experiments, the rigid plastic housing is used for shaping. In the multi-layer experiment, the soft skin with fat

is used for shaping. Obviously, in the multi-layer experiment, deformation arises more easily. The more the number of experiments is, the more obvious deformation is. Meanwhile, as the experiment time is prolonged, dehydration will occur in the flexible skin experiment. This causes data of similar multiple experiments at the same position in three consecutive days (twenty-hour interval) to have larger error than those in the single-layer experiment and the bi-layer experiment (about 4dB). For this reason, in future research, the effect of deformation should be taken into account.

According to experimental results, we find that the path attenuation of the ITO channel is greater than that of the OTI channel. When the signal is transmitted from inside to outside, there is electric current distributed on the six surfaces of the implantable device; while current distribution only exists on the surface (contacting with the electrode) of the surface device when the signal is transmitted from outside to inside. The signal intensity of the ITO channel is significantly higher than that of the OTI channel, and the path attenuation of the ITO channel is inevitably greater than that of the OTI channel.

In the modeling, because we assume that the potentials on the top and the bottom surfaces are 0, so in the process of model calculation, the closer it gets to the bottom surface, the closer to 0 the model result is; this is somewhat different from the boundary of the physical field in this experiment. For this reason, so we will further improve the boundary condition in the next step.

Additionally, in the experimental verification, whether in physiological saline experiment or in Muscle with Bone Effect Experiment, we construct an isotropic volume conductor, so this has some difference with actual structure of human tissues. In future research, we will do further research on anisotropic aspect.

V. CONCLUSION

This paper presents a mathematical model of a multi-layer volume conductor for analyzing signal path gain characteristics that affect implantable electronic devices at any location in the human body. Within the operational frequency range that satisfies the quasi-static standard approximation, we used the volume conductor theory, Maxwell's equations, and the Poisson's equation to derive a governing equation of the electric potential distribution of the implantable communication carrier's surface. To enhance the model's accuracy, the permittivity is used at the initial stage of modeling. Thus, the model also reflects the capacitance effect.

Because experimental verification of the model on a human body was not possible due to procedural challenges, physiological saline and Muscle with Bone effect experiment were used to verify the model. In the physiological saline experiment, when we input a sinusoidal signal of 0 dBm at 100 kHz, the difference between the calculated and experimental results was less than 2 dB. In the Muscle with Bone effect experiment, when we input a sinusoidal signal of 0 dBm at 100 kHz, the path loss difference between the calculated and experimental results was less than 1.6 dB and 4 dB, respectively. Therefore, the proposed model is considered sufficiently accurate to be practically applicable.

In the model, the tissues were considered to be isotropic for simplicity. This assumption is only an approximation of the real tissues, especially because of the differences between the transverse and parallel properties of muscle tissues. For this reason, in the future, we will further analyze the effects of tissue characteristics and geometries on the model to improve its precision.

TABLE 7. Bi-layer experiment fitting parameters.

Fitting	Distance experiment(Figure. 10)			
Equation	$y = b_0 + b_1 * x^1 + b_2 * x^2$			
Mode	ITO		OTI	
RSS	11.41234		17.9382	
R-Square	0.99776		0.99602	
	Value	SE	Value	SE
b_0	-17.78997	0.41919	-25.12285	0.52555
b_1	-0.24475	0.00984	-0.29718	0.01223
b_2	-1.31739E-4	5.42284E-5	2.51035E-4	6.79875E-5
Fitting	Depth experiment(Figure. 11)			
Equation	$y = b_0 + b_1 * x^1 + b_2 * x^2$			
Mode	ITO		OTI	
RSS	7.80666		9.58973	
R-Square	0.9059		0.89941	
	Value	SE	Value	SE
b_0	-33.33119	0.67976	-41.49326	0.7534
b_1	0.09299	0.0575	-0.15137	0.06373
b_2	-0.00136	0.00114	-4.18769E-4	0.00127

*SE:Standard Error, RSS:Residual Sum of Squares

TABLE 8. Multi-layer experiment fitting parameters.

Fitting	Distance experiment(Figure. 13)			
Equation	$y = b_0 + b_1 * x^1 + b_2 * x^2$			
Mode	ITO		OTI	
RSS	71.87678		57.67706	
R-Square	0.98919		0.98956	
	Value	SE	Value	SE
b_0	-20.65352	1.05201	-30.86277	0.94238
b_1	-0.30943	0.02469	-0.30882	0.02212
b_2	2.42411E-5	1.36092E-4	1.70221E-4	1.2191E-4
Fitting	Depth experiment(Figure. 14)			
Equation	$y = b_0 + b_1 * x^1 + b_2 * x^2$			
Mode	ITO		OTI	
RSS	60.77927		94.13252	
R-Square	0.9489		0.9378	
	Value	SE	Value	SE
b_0	-39.83441	0.92282	-47.20141	1.14844
b_1	0.07672	0.06616	-0.0209	0.08234
b_2	-0.00737	0.00109	-0.00653	0.00136

*SE:Standard Error, RSS:Residual Sum of Squares

APPENDIX

See Tables 5–8.

REFERENCES

[1] M. Velliste, S. Perel, M. C. Spalding, A. S. Whitford, and A. B. Schwartz, "Cortical control of a prosthetic arm for self-feeding," *Nature*, vol. 453, no. 7198, pp. 1098–1101, Jun. 2008.

[2] C. T. Moritz, S. I. Perlmutter, and E. E. Fetz, "Direct control of paralysed muscles by cortical neurons," *Nature*, vol. 456, pp. 639–643, Dec. 2008.

[3] M. A. L. Nicolelis, "Actions from thoughts," *Nature*, vol. 409, pp. 403–407, Jan. 2001.
[4] G. E. Loeb, F. J. R. Richmond, W. H. Moore, and R. A. Peck, "Design and fabrication of hermetic microelectronic implants," in *Proc. 1st Annu. Int. Conf. Microtechnol. Med. Biol.*, Oct. 2000, pp. 455–459.
[5] J. E. Ferguson and A. D. Redish, "Wireless communication with implanted medical devices using the conductive properties of the body," *Expert Rev. Med. Devices*, vol. 8, no. 4, pp. 427–433, 2011.
[6] E. Zrenner, "Will retinal implants restore vision?" *Science*, vol. 295, pp. 1022–1025, Feb. 2002.
[7] W. Germanovix and C. Toumazou, "Design of a micropower current-mode log-domain analog cochlear implant," *IEEE Trans. Circuits Syst. II, Analog Digit. Signal Process.*, vol. 47, no. 10, pp. 1023–1046, Oct. 2000.
[8] P. C. Laizou, "Signal-processing techniques for cochlear implants," *IEEE Eng. Med. Biol. Mag.*, vol. 18, no. 3, pp. 34–46, May 1999.
[9] A. L. Benabid, S. Chabardes, J. Mitrofanis, and P. Pollak, "Deep brain stimulation of the subthalamic nucleus for the treatment of Parkinson's disease," *Lancet Neurol.*, vol. 8, no. 1, pp. 67–81, 2009.
[10] N. Miura, D. Mizoguchi, T. Sakurai, and T. Kuroda, "Analysis and design of inductive coupling and transceiver circuit for inductive inter-chip wireless superconnect," *IEEE J. Solid-State Circuits*, vol. 40, no. 4, pp. 829–837, Apr. 2005.
[11] "Electromagnetic compatibility and radio spectrum matters (ERM); Radio equipment in the frequency range 402 MHz to 405 MHz for ultra-low power active medical implants and accessories, Part 1: Technical characteristics, including electromagnetic compatibility requirements, and test methods," European Telecommun. Standards Inst., Sophia Antipolis, France, Tech. Rep. ETSI EN 301 839-1 V1.3.1 (2009-10), 2002.
[12] T. G. Zimmerman, "Personal area networks (PAN): Near-field intra-body communication," M.S. thesis, Dept. Humanities Eng., MIT, Cambridge, MA, USA, 1995.
[13] N. Haga, K. Saito, M. Takahashi, and K. Ito, "Proper derivation of equivalent-circuit expressions of intra-body communication channels using quasi-static field," *IEICE Trans. Commun.*, vol. E95, no. 1, pp. 51–59, 2012.
[14] K. Hachisuka *et al.*, "Simplified circuit modeling and fabrication of intra-body communication devices," *Sens. Actuators A, Phys.*, vols. 130–131, pp. 322–330, Aug. 2006.
[15] Y. Song, Q. Hao, K. Zhang, M. Wang, Y. Chu, and B. Kang, "The simulation method of the galvanic coupling intrabody communication with different signal transmission paths," *IEEE Trans. Instrum. Meas.*, vol. 60, no. 4, pp. 1257–1266, Apr. 2011.
[16] N. Haga, K. Saito, M. Takahashi, and K. Ito, "Equivalent circuit of intrabody communication channels inducing conduction currents inside the human body," *IEEE Trans. Antennas Propag.*, vol. 61, no. 5, pp. 2807–2816, May 2013.
[17] M. S. Wegmueller *et al.*, "An attempt to model the human body as a communication channel," *IEEE Trans. Biomed. Eng.*, vol. 54, no. 10, pp. 1851–1857, Oct. 2007.
[18] M. S. Wegmüller, "Intra-body communication (IBC) for biomedical sensor networks," Ph.D. dissertation, ETH, Zürich, Switzerland, 2007.
[19] Y. Song, K. Zhang, Q. Hao, L. Hu, J. Wang, and F. Shang, "A finite-element simulation of galvanic coupling intra-body communication based on the whole human body," *Sensors*, vol. 12, no. 10, pp. 13567–13582, 2012.
[20] S. H. Pun, Y. M. Gao, P. U. Mak, M. I. Vai, and M. Du, "Quasi-static modeling of human limb for intra-body communications with experiments," *IEEE Trans. Inf. Technol Biomed.*, vol. 15, no. 6, pp. 870–876, Nov. 2011.
[21] X. M. Chen *et al.*, "Study of channel characteristics for galvanic-type intra-body communication based on a transfer function from a quasi-static field model," *Sensors*, vol. 12, no. 12, pp. 16433–16450, 2012.
[22] R. Plonsey and D. B. Heppner, "Considerations of quasi-stationarity in electrophysiological systems," *Bull. Math. Biol.*, vol. 29, no. 4, pp. 657–664, 1967.
[23] D. Farina, L. Mesin, S. Martina, and R. Merletti, "A surface EMG generation model with multilayer cylindrical description of the volume conductor," *IEEE Trans. Biomed. Eng.*, vol. 51, no. 3, pp. 415–426, Mar. 2004.
[24] P. R. Wallace, *Mathematical Analysis of Physical Problems*. New York, NY, USA: Dover, 1984.
[25] C. Gabriel, S. Gabriel, and E. Corthout, "The dielectric properties of biological tissues: I. Literature survey," *Phys. Med. Biol.*, vol. 41, no. 11, p. 2231, 1996.
[26] S. Gabriel, R. W. Lau, and C. Gabriel, "The dielectric properties of biological tissues: II. Measurements in the frequency range 10 Hz to 20 GHz," *Phys. Med. Biol.*, vol. 41, no. 11, p. 2251, 1996.
[27] C. Gabriel, A. Peyman, and E. H. Grant, "Electrical conductivity of tissue at frequencies below 1 MHz," *Phys. Med. Biol.*, vol. 54, no. 16, p. 4863, 2009.
[28] T. Karacolak, R. Cooper, E. S. Unlu, and E. Topsakal, "Dielectric properties of porcine skin tissue and *in vivo* testing of implantable antennas using pigs as model animals," *IEEE Antennas Wireless Propag. Lett.*, vol. 11, pp. 1686–1689, 2012.
[29] M. Swaminathan, F. S. Cabrera, J. S. Pujol, U. Muncuk, G. Schirner, and K. R. Chowdhury, "Multi-path model and sensitivity analysis for galvanic coupled intra-body communication through layered tissue," *IEEE Trans. Biomed. Circuits Syst.*, vol. 10, no. 2, pp. 339–351, Apr. 2016.
[30] E. Y. Chow, Y. H. Ouyang, B. Beier, W. J. Chappell, and P. P. Irazoqui, "Evaluation of cardiovascular stents as antennas for implantable wireless applications," *IEEE Trans. Microw. Theory Techn.*, vol. 57, no. 10, pp. 2523–2532, Oct. 2009.
[31] F. L. H. Gielen, W. Wallinga-de Jonge, and K. L. Boon, "Electrical conductivity of skeletal muscle tissue: Experimental results from different muscles *in vivo*," *Med. Biol. Eng. Comput.*, vol. 22, pp. 569–577, Nov. 1984.
[32] M. A. Callejón, P. del Campo, J. Reina-Tosina, and L. M. Roa, "A parametric computational analysis into galvanic coupling intrabody communication," *IEEE J. Biomed. Health Informat.*, vol. 22, no. 4, pp. 1087–1096, Jul. 2018.
[33] D. Naranjo-Hernández, A. Callejón-Leblic, Z. L. Vasić, M. Seyedi, and Y.-M. Gao, "Past results, present trends, and future challenges in intra-body communication," *Wireless Commun. Mobile Comput.*, vol. 2018, Mar. 2018, Art. no. 9026847.
[34] J. F. Zhao, X. M. Chen, B. D. Liang, and Q. X. Chen, "A review on human body communication: Signal propagation model, communication performance, and experimental issues," *Wireless Commun. Mobile Comput.*, vol. 2017, Oct. 2017, Art. no. 5842310.
[35] S. Lin *et al.*, "Biological evaluation of the effect of galvanic coupling intra-body communication on human skin fibroblast cells," *Wireless Commun. Mobile Comput.*, vol. 2017, Sep. 2017, Art. no. 8674035.
[36] M. A. Callejón, J. Reina-Tosina, D. Naranjo-Hernández, and L. M. Roa, "Galvanic coupling transmission in intrabody communication: A finite element approach," *IEEE Trans. Biomed. Eng.*, vol. 61, no. 3, pp. 775–783, Mar. 2014.

SHUANG ZHANG (S'15) received the B.S. degree in mathematics and applied mathematics from Neijiang Normal University, Neijiang, China, in 2007, and the M.S. degree in control engineering from the Institute of Optics and Electronics, Chinese Academy of Sciences, Chengdu, in 2011. He is currently pursuing the Ph.D. degree in electrical and computer engineering with the University of Macau, Macau, China.

He has been an Assistant Professor with the College of Computer Science, Neijiang Normal University. His current research interests include human body communication, digital signal processing, and body sensor networks.

SIO HANG PUN received the master's degree in computer and electrical engineering from the University of Porto, Portugal, in 1999, and the Ph.D. degree in electrical and electronics engineering from the University of Macau, Macau, in 2012.

Since 2012, he has been an Associate Professor with the State Key Laboratory of Analog and Mixed-Signal VLSI, University of Macau. His current research interests include biomedical electronic circuits, miniaturized sensors for biomedical applications, and human body communication.

PENG UN MAK (S'88–M'97–SM'11) received the B.Sc. degree in electrical engineering from National Taiwan University, Taipei, Taiwan, and the M.Sc. and Ph.D. degrees in electrical engineering from Michigan State University, East Lansing, MI, USA. Since 1997, he has been an Assistant Professor with the Department of Electrical and Computer Engineering, University of Macau, Macau, China. He has authored or co-authored over 150 peer-reviewed technical publications, including journals, book chapters, and conference proceedings. He has performed research in biosignal extraction and processing, bioelectromagnetism, human body communication, and body sensor networks. He was a Visiting Fellow of the University of Cambridge at Clare Hall, Cambridge, U.K., in 2018. He is a currently a Life Member of the Phi Kappa Phi and an Invited Member of the Eta Kappa Nu (currently IEEE-HKN).

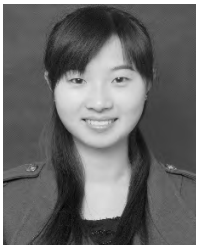

YU PING QIN received the B.S. degree in mathematics and applied mathematics from Neijiang Normal University, Neijiang, China, in 2008, and the M.S. degree in probability theory and mathematical statistics from Sichuan Normal University, in 2011.

She has been an Assistant Professor with the College of Computer Science, Neijiang Normal University. Her current research interests include human body communication, digital signal processing, and digital image processing.

YI HE LIU received the Ph.D. degree in applied mathematics from Sichuan University, Chengdu, Sichuan, China, in 2005. Since 2009, he has been performing research in the area of intra-body communication. He is currently a Professor with the College of Computer Science, Neijiang Normal University.

YUE MING GAO received the Ph.D. degree in electrical engineering from Fuzhou University, Fuzhou, China, in 2010. Since 2004, he has been performing research in the areas of bioelectromagnetism and biomedical signal detecting technology. He is currently a Professor with the College of Physical and Information Engineering, Fuzhou University.

MANG I VAI (M'92–SM'06) received the Ph.D. degree in electrical and electronics engineering from the University of Macau, China, in 2002. Since 1984, he has been performing research in the areas of digital signal processing and embedded systems. He is currently the Coordinator of the State Key Laboratory of Analog and Mixed-Signal VLSI and an Associate Professor of electrical and computer engineering with the Faculty of Science and Technology, University of Macau.